actuators

MDPI

Communication

Dynamic Analysis of Intermittent-Motion Conveyor Actuator

Alexander Prikhodko

Land Transport and Mechanics Department, Kuban State Technological University, 350072 Krasnodar, Russia; sannic92@gmail.com; Tel.: +7-861-255-97-43

Abstract: Conveyors are one of the important components of transport systems and are used in almost all branches of mechanical engineering. This paper investigates the dynamics of the intermittent motion conveyor mechanical system. The mechanical transmission is a planetary mechanism with elliptical gears, in which the intermittent motion of the output shaft is provided by a variable gear ratio of non-circular gears. A single-mass dynamic model is built by reducing the masses, forces and moments to the initial link, which is the input shaft of the mechanism. The solutions of the equations of initial link motion were obtained using two methods, the energy-mass method and the third-order Hermite method. Dynamic studies by the energy-mass method made it possible to determine flywheel moment of inertia to reduce the coefficient of initial link rotation irregularity. The convergence of the functions of the initial link angular velocity obtained by both methods was confirmed. The results can be used for further force analysis, strength calculations, design and manufacture of the conveyor.

Keywords: intermittent motion; planetary gear; elliptical gears; dynamic analysis; mechanical actuator design

Citation: Prikhodko, A. Dynamic Analysis of Intermittent-Motion Conveyor Actuator. *Actuators* **2021**, *10*, 174. https://doi.org/10.3390/act10080174

Academic Editors: Hai Wang, Ming Yu, Zhaowu Ping, Yongfu Li and Bin Xu

Received: 3 June 2021
Accepted: 22 July 2021
Published: 24 July 2021

1. Introduction

Transportation structures consisting of conveyors and their systems are widely used in various branches of modern industry: coal, mining, electric power, machining, chemical, food and many other fields [1–3]. Belt conveyors have become widespread due to their high loading capacity, speed and the possibility of transportation over long distances [4,5]. The belt is the weakest link of conveyor, therefore, a large number of papers are devoted to the strength calculations of the belt [6–10], as well as the diagnostics of belt conveyors using inspection robots [11] and computer vision [12–15].

For the purpose of rational mechanical design and operation of conveyors, much attention of researchers should also be paid to other components of drive systems: bearings [16], gearboxes [17], idlers [18]. The design of the conveyor actuator is currently a relatively well-known and widely studied problem, especially in the particular case when the conveyor belt moves at a constant speed. However, many production lines require stopping the conveyor belt for various operations on the product, and this issue can be solved using mechanical drives of intermittent motion.

The intermittent motion mechanisms make it possible to have the required duration stops of the output link with constant angular velocity of the input link [19]. The mechanical system "electric motor—actuator—working element (for example, a conveyor pulley)" is rational construction, since the motor operates in the most efficient constant mode, and the efficiency of the mechanical transmission is high. The most common type of mechanical device for the implementation of intermittent movement is the Maltese cross (Geneva drive) [20]. Although it has been researched and modernized [21,22] over the decades, the Geneva drive has a significant disadvantage. Intermittent movement in such mechanisms is provided due to the rupture of the kinematic chain, which leads to shocks that occur at the beginning and end of the movement phase [23].

In recent years, scholars have been increasing their attention to the research of mechanical transmissions with non-circular gears as the most effective method for realizing nonlinear transfer functions [24–26]. This type of mechanical transmission also makes it possible to realize the intermittent motion of the output link without breaking the kinematic chain. Non-circular gears can have various shapes, but the most common are elliptical ones [27–29]. This is mainly due to extensive studies of their geometry and kinematics [30,31], the solution of various problems of their manufacture [32,33].

An important place in the study of machines and actuators is given to the study of their dynamics, which makes it possible to find the laws of motion of the machine parts, to perform analysis of the forces acting on the working bodies, to identify irrationally functioning units, to investigate and optimize the operating modes of the device, as well as the overall design [34–37]. However, most of the papers on the creation of non-circular gears are devoted only to the geometry and kinematics of these mechanisms, while the issues of their dynamics are much more complex and not studied. Nevertheless, some applied problems of the dynamics of non-circular gears have been solved. For example, Xing Liu et al. [38] carried out a theoretical and experimental study of the dynamic performance of elliptical gears with rotational axes at the focus and center of the pitch ellipse. Nan Gao et al. [29] investigated parametric vibrations and instabilities of elliptical gears caused by loading torque and eccentricity vibrations. Zhiqin Cai and Chao Lin [39] presented and investigated a generalized nonlinear dynamic model of a curved gear drive based on Lagrange–Bondon graphs. Many researchers have considered the issues of dynamics in relation to practical applications of mechanical devices [38–40] containing non-circular gears, since dynamic models include the parameters of the technological load on the working body of the machine.

Complex nonlinear functions of fluctuations in the speed oflinks of cyclic mechanisms, which also include transmissions by non-circular gears, lead to irregular movement of the input (initial) link of the mechanism, to which the motor shaft is connected directly or through a gearbox. Speed fluctuations on the motor shaft cause vibrations of the machine body, and cause noise, vibration, and reduced drive reliability. Therefore, in this study, it is proposed to construct and study a single-mass dynamic model of the intermittent-motion conveyor actuator in order to determine the function of the angular velocity of the initial link, identify the irregularity of its motion and determine the inertial characteristics of the flywheel to reduce the coefficient of irregularity to the permissible values.

2. Description of the Conveyor Actuator Mechanical System and Problem Statement

The object of research is the conveyor actuator; a simplified scheme (Figure 1) includes the electric motor 1, planetary mechanism of intermittent motion 2, and a working body 3 (drive pulley of conveyor). In the considered schematic, the motor shaft is connected directly to the input shaft of the planetary mechanism, and the axis of the drive pulley is rigidly connected to the output shaft.

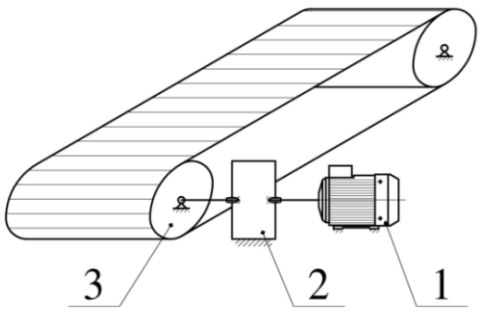

Figure 1. Scheme of the conveyor actuator.

Intermittent motion of the conveyor pulley is ensured by mechanically converting the uniform rotational motion of the input shaft into non-uniform motion with stops of the output shaft. The design of the planetary gear with elliptical gears, which allows this transformation, is considered in [31] and is shown in Figure 2.

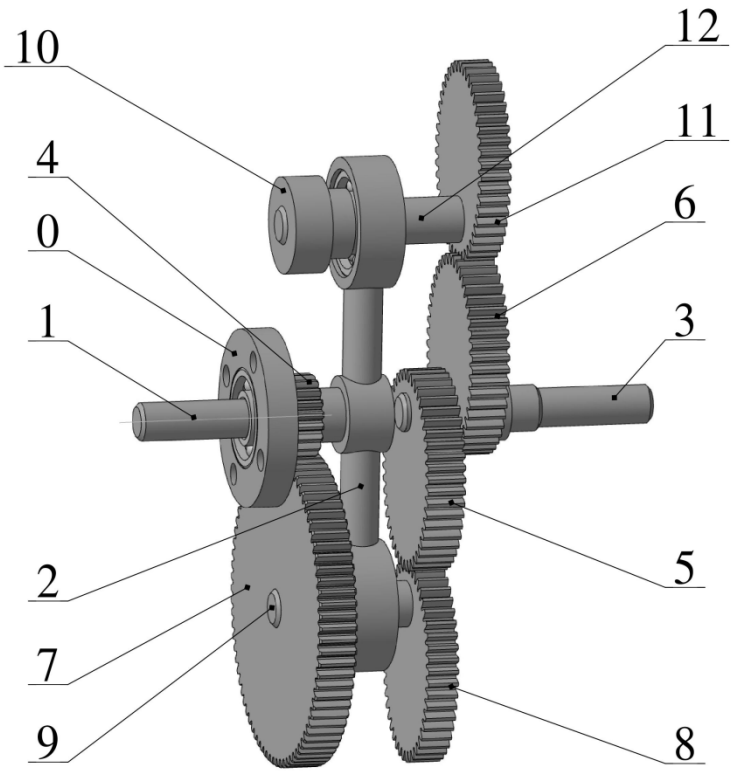

Figure 2. Intermittent motion planetary mechanism with elliptical gears.

The rotation of the motor shaft is transmitted to the input shaft 1 and the carrier 2. The rotational movement of the carrier causes the spur gear 7 to roll around the fixed gear 4. Motion of the spur gear 7 is transmitted to the satellite shaft 9 and the elliptical gear 8, which drives the elliptical gear 5 and, accordingly, the output shaft 3. At the moment when the gear ratio of the pair of elliptical wheels is equal to the gear ratio of the pair of circular wheels, the output shaft 3 stops. Further, the speed of the output shaft increases to a maximum value, then decreases again to zero, which leads to an intermittent motion of the output shaft. Intermittent motion of the output link is provided in a special case: the radius of the circular gear must meet one of two conditions: $R = a - c$ or $R = a + c$, where a and c are semi-major axis and focal distance of the pitch ellipse [31]. The second satellite, containing the counterweight 10, the elliptical gear 11 and the shaft 12, is necessary to balance the mechanism [41] and repeats the movement of the first satellite. Intermittent motion is transmitted to the driving pulley, which drives the conveyor belt and the driven pulley. Since the output shaft of the planetary mechanism rotates with stops, the load on the conveyor belt will move in translational motion with stops.

The planetary actuator has one degree of freedom, and its links are rigidly connected to each other, therefore, to solve the set problem, it is advisable to replace the real mechanism with a single-mass dynamic model, taking input shaft 1 as the reduction link. The equation of motion of the driving link for a mechanical system with one degree of freedom has the following form [42]:

$$\frac{\omega_1^2}{2} \cdot \frac{dI_r}{d\varphi_1} + \varepsilon_1 \cdot I_r = M_{rr} + M_{rd} \quad (1)$$

where φ_1, ω_1, ε_1 are the rotation angle, angular velocity and angular acceleration of the reduction link 1, I_r is reduced to link 1 moment of inertia, M_{rr} is reduced to link 1 resistance moment, M_{rd} is reduced to link 1 driving moment.

The aim of the work is not only to find the law of motion of the reduction link $\omega_1(t)$, but also to conduct a deeper dynamic analysis of the mechanical system, namely, to find the driving moment, the moment of inertia of the flywheel and reduce the rotation irregularity of the drive link. Therefore, to study the obtained dynamic model, a simpler and more visual energy-mass method is used, and the verification of the obtained solutions is carried out using a numerical method, the third-order Hermite interpolation function [43].

3. Description and Construction of a Dynamic Model

3.1. Reduced Inertia Moment

The parameter characterizing the mass-inertial characteristics of the mechanism, taking into account its kinematics, is the reduced moment of inertia [42]:

$$I_r = \sum_{i=1}^{n} m_i S'^2_i + \sum_{i=1}^{n} I_{S_i} \varphi'^2_i, \quad (2)$$

where n is the number of movable links in which masses and moments of inertia are known; m_i is the mass of the i-th link; I_{S_i} is the moment of inertia of the i-th link relative to the axis passing through the center of mass; $S'_i = \frac{dS_i}{d\varphi_1}$ is the velocity analogue of the center of mass of the i-th link; $\varphi'_i = \frac{d\varphi_i}{d\varphi_1}$ is the angular velocity analogue of the of the i-th link.

Equation (2) for the investigated mechanical system will take the form:

$$\begin{gathered} I_r = I_m + I_1 + I_2 + (m_7 + m_9 + m_{10} + m_{12}) \cdot S'^2_9 + (m_8 + m_{11}) \cdot S'^2_8 + \\ (I_7 + I_8 + I_9 + I_{10} + I_{11} + I_{12}) \cdot \varphi'^2_9 + (I_3 + I_5 + I_6 + I_{wb}) \cdot \varphi'^2_3, \end{gathered} \quad (3)$$

where I_m is the moment of inertia of the motor; I_{wb} is the moment of inertia of the working body. The moments of inertia and velocity analogues of the actuator links are designated in accordance with Figure 2.

Differentiating (3) with respect to the generalized coordinate φ_1, we obtain:

$$\begin{gathered} \frac{dI_r}{d\varphi_1} = 2 \cdot [(m_7 + m_9 + m_{10} + m_{12}) \cdot S'_9 \cdot S''_9 + (m_8 + m_{11}) \cdot S'_8 \cdot S''_8 + \\ (I_7 + I_8 + I_9 + I_{10} + I_{11} + I_{12}) \cdot \varphi'_9 \cdot \varphi''_9 + (I_3 + I_5 + I_6 + I_{wb}) \cdot \varphi'_3 \cdot \varphi''_3]. \end{gathered} \quad (4)$$

The functions of linear and angular velocities analogues, describing the kinematics of the mechanism and included in Equations (3) and (4), are determined using the plan of the velocities [44] of the mechanism links (Figure 3).

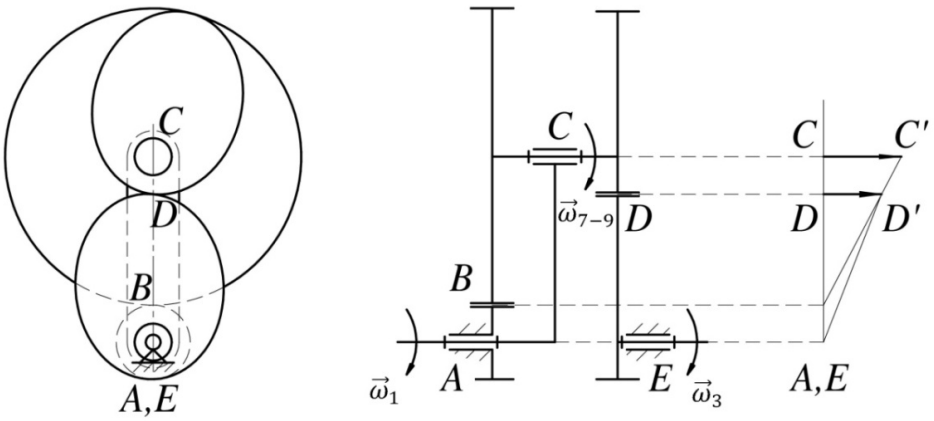

Figure 3. Plan of the mechanism velocities.

The analogue of the angular velocity of the output link 3, according to Figure 3, is defined as:

$$\varphi'_3 = \frac{\omega_3}{\omega_1} = \frac{V_D \cdot AC}{V_C \cdot DE}, \quad (5)$$

where V_D and V_C are the velocities of points D and C, AC and DE are the lengths of the segments in Figure 3.

Considering that $\frac{V_D}{V_C} = \frac{BD}{BC}$ from the similarity of the triangles BDD' and BCC', we obtain the following:

$$\varphi'_3 = \frac{BD \cdot AC}{BC \cdot DE}. \quad (6)$$

The distances AC and BC in Equation (6) are determined as:

$$AC = R_1 + R_2; \quad (7)$$

$$BC = R_2, \quad (8)$$

where R_1 is the radius of the sun wheel 4, R_2 is the radius of the cylindrical wheel 6 of the satellite.

The lengths of the segments BD and DE are determined through the length of the segment CD, which is found using the equation of the centroid of the elliptical wheel [45]:

$$CD = \rho = \frac{a \cdot (1 - e^2)}{1 + e \cdot \cos \varphi_8}, \quad (9)$$

where $\varphi_8 = \frac{R_1}{R_2}\varphi_1$ is the angle of rotation of the elliptical wheel 8; a, e are semi-major axis and eccentricity of the pitch ellipse.

Then, according to Figure 3, the segments BD and DE are defined as:

$$BD = BC - CD; \quad (10)$$

$$DE = AC - CD. \quad (11)$$

Substituting (7)–(11) into (6), we obtain an equation for determining the analogue of the output shaft angular velocity:

$$\varphi'_3 = 1 - \frac{R_1 \rho}{R_2(R_1 + R_2 - \rho)}. \quad (12)$$

Also, to construct a dynamic model, it is necessary to determine the analogue of the angular velocity of the satellite φ'_9 and analogues of the linear velocities of the centers of mass of links 7, 9 (point C in Figure 4) S'_9 and link 8 (point K in Figure 4) S'_8.

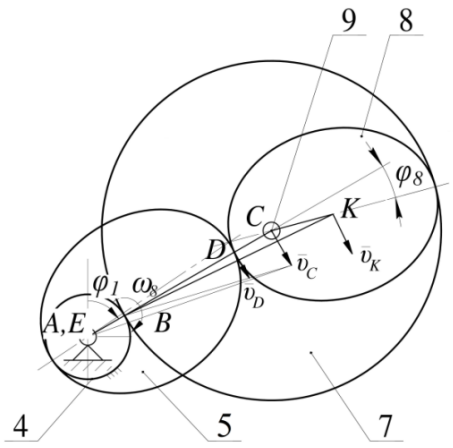

Figure 4. Scheme for determining the velocities V_C and V_K.

Velocity analogues are determined as follows:

$$S'_9 = \frac{V_C}{\omega_1} = \frac{\omega_1 \cdot AC}{\omega_1} = R_1 + R_2; \tag{13}$$

$$\varphi'_9 = \frac{\omega_9}{\omega_1} = \frac{V_C}{R_2 \cdot \omega_1} = \frac{S'_9}{R_2} = \frac{R_1 + R_2}{R_2}; \tag{14}$$

$$S'_8 = \frac{V_K}{\omega_1} = \frac{\omega_9 \cdot BK}{\omega_1} = \varphi'_9 \cdot BK = \frac{(R_1 + R_2) \cdot BK}{R_2}. \tag{15}$$

The segment BK is determined from the triangle BCK (Figure 4):

$$BK = \sqrt{(a \cdot e)^2 + R_2^2 - 2 \cdot a \cdot e \cdot R_2 \cdot \cos \varphi_8}. \tag{16}$$

Thus, the obtained equations of kinematics (12)–(16) make it possible to determine, using (3), (4), the reduced moment of inertia of the mechanism and its derivative.

3.2. Reduced Moment of Resistance Forces

An important parameter used in Equation (1) and characterizing the operation of the considered mechanical system is the reduced moment of resistance (M_{rr}). It takes into account the work of all external forces and moments (excluding the driving moment) acting on the machine: forces and moments of useful resistance forces, forces and moments of harmful resistance, gravity forces. The reduced moment of resistance forces, in the general case, is defined as:

$$M_{rr} = \sum_{i=1}^{n} \left(\sum_{i=1}^{m} F_i \cdot S'_i + \sum_{i=1}^{q} M_i \cdot \varphi'_i \right), \tag{17}$$

where n is the total number of moving links; m is the number of forces F acting on the i-th link; S'_i is the velocity analogue of the force point of application; q is the number of moments M acting on the i-th link.

The forces of harmful resistance are the forces of friction acting in the kinematic pairs of the mechanism: bearings, gearing, etc. Determination of these forces is a rather difficult task, and their values are small in comparison with other resistance forces, therefore, in the conditions of the studied mechanical system, the friction forces were not taken into account.

The design scheme for determining works of the gravity forces acting on the links of the mechanism is shown in Figure 5.

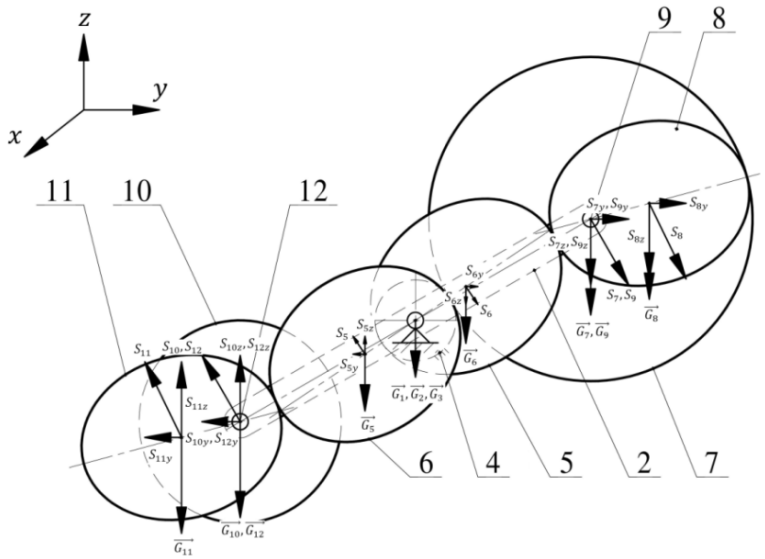

Figure 5. Scheme for determining works of the gravity forces.

As can be seen from Figure 5, the axes of rotation of all links are parallel to the horizontal plane *Oxy*. The gravity forces of the links with the centers of mass on the fixed axes ($\vec{G}_1$, $\vec{G}_2$, $\vec{G}_3$) do not perform work, since the vertical displacement in this case is equal to zero. The forces of gravity applied to the centers of mass of the satellites and elliptical gears will perform work, which is defined as:

$$A_G = \sum m_i g \cdot S_{iz}, \tag{18}$$

where m_i is the mass of the i-th link, S_{iz} is the displacement of the i-th link along the z axis. The masses of the links lying on the opposite satellites are equal, from the conditions of balancing the mechanism [41], and the displacements along the z-axis are equal in module, but have opposite directions. Thus, the sum of the work of all gravity forces in the investigated mechanical system will be equal to zero.

A useful resistance acts on the working body of the investigated mechanical system (the drive pulley of the conveyor), which is taken into account in the dynamic model and affects the laws of motion of the links of the mechanism. It is assumed that there is a load of constant mass on the conveyor belt, and the useful resistance is modeled by a constant moment M = 4.67 nm.

Thus, since only the moment of resistance acts on the working body in the investigated device, then Equation (17) for determining the reduced moment of resistance will take the form:

$$M_{rr} = M_r \cdot \varphi'_3. \tag{19}$$

3.3. Initial Parameters for Dynamic Analysis

As an example, a conveyor with the following parameters was investigated (the numbers of the links correspond to Figure 2): I_m = 100 $g \cdot cm^2$ (motor); I_1 = 9.8 $g \cdot cm^2$; I_2 = 600 $g \cdot cm^2$; I_3 = 30.4 $g \cdot cm^2$; $I_5 = I_6$ = 627 $g \cdot cm^2$; I_7 = 998 $g \cdot cm^2$, m_7 = 0.39 kg; $I_8 = I_{11}$ = 564 $g \cdot cm^2$, $m_8 = m_{11}$ = 0.09 kg; I_9 = 19.2 $g \cdot cm^2$, m_9 = 0.04 kg; I_{10} = 972 $g \cdot cm^2$, m_{10} = 0.38 kg; I_{12} = 25 $g \cdot cm^2$, m_{12} = 0.05 kg; I_{wb} = 1500 $g \cdot cm^2$ (working body); R_1 = 40 mm, R_2= 10 mm, a = 25 mm, e = 0.6; permissible coefficient of rotation irregularity [δ] = 0.05. The input shaft of the actuator is driven by a motor whose rotation speed ω_1 = 157 rad/s (n_1 = 1500 rpm).

4. Numerical Modeling Results

Integrating (12) over the generalized coordinate φ_1, we obtain a graph of the dependence of the angle of rotation of the output shaft φ_3 on the angle of rotation of the input shaft φ_1 (Figure 6).

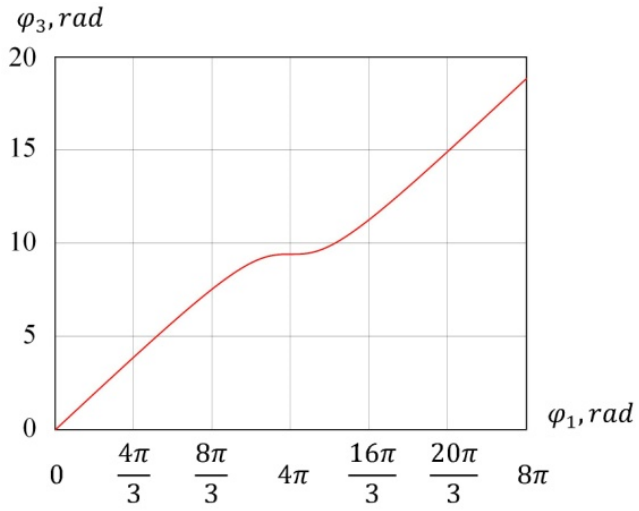

Figure 6. Graph of function $\varphi_3(\varphi_1)$.

As shown on the graph in Figure 6, the output shaft makes one stop every four revolutions of the input shaft. According to Equations (3) and (4), the graphs of the functions of the reduced moment of inertia I_r and its derivative $\frac{dI_r}{d\varphi_1}$ from the angle of rotation of the input link φ_1, taking into account given initial parameters, are plotted in Figure 7.

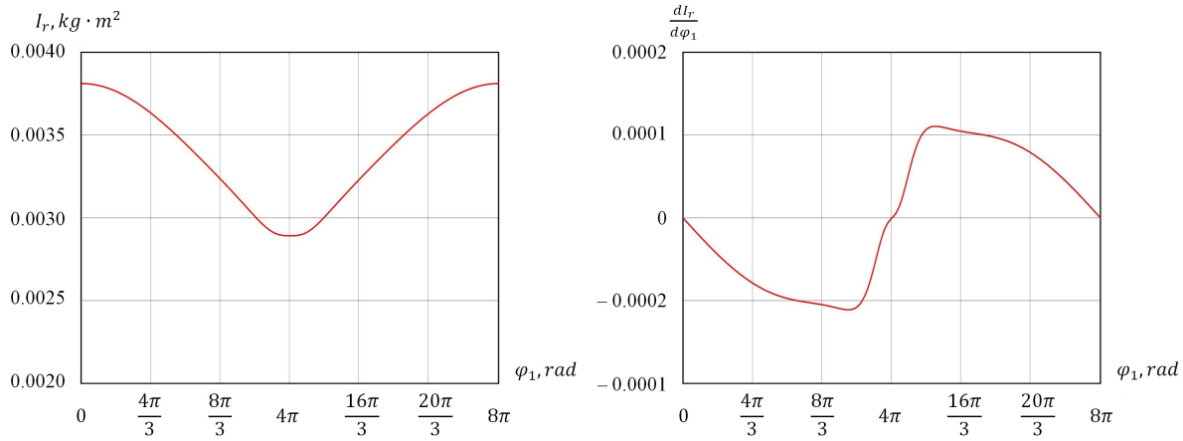

Figure 7. Graphs of functions $I_r(\varphi_1)$, $\frac{dI_r}{d\varphi_1}(\varphi_1)$.

In accordance with the energy-mass method, the increment of kinetic energy ΔT is determined as follows:

$$\Delta T = A_d - A_r, \tag{20}$$

where A_d is the work of the driving moment, A_r is the work of the moment of resistance.

The works in Equation (20) will be determined as:

$$A_d = M_{rd} \cdot \varphi_1; \tag{21}$$

$$M_{rd} = \frac{\int_0^{2\pi} M_{rr} d\varphi_1}{2\pi}; \tag{22}$$

$$A_r = \int_0^{\varphi_1} M_{rr} d\varphi_1. \tag{23}$$

Using Equations (20)–(23), the graphs of the functions A_r, A_d, ΔT were obtained (Figure 8).

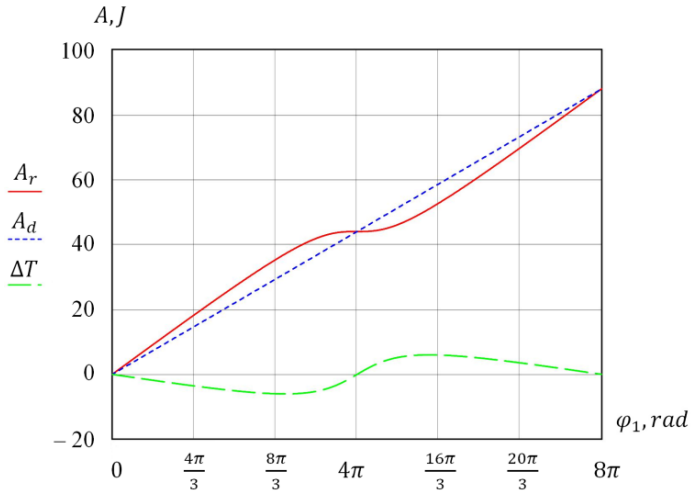

Figure 8. Graphs of functions $A_r(\varphi_1)$, $A_d(\varphi_1)$, $\Delta T(\varphi_1)$.

The angular velocity of the reduction link will be determined as [42]:

$$\omega_1 = \sqrt{\frac{2\Delta T - C_{max} - C_{min}}{I_r}}, \tag{24}$$

where C_{max} and C_{min} are determined as:

$$C_{max} = max\left[\Delta T - \frac{1}{2} I_r \omega_{av}^2 (1 + [\delta])\right]; \tag{25}$$

$$C_{min} = min\left[\Delta T - \frac{1}{2} I_r \omega_{av}^2 (1 - [\delta])\right]. \tag{26}$$

Using (24)–(26) and the calculation results (Figures 7 and 8), the function $\omega_1(\varphi_1)$ was obtained. Substituting the initial data and values of M_{rd} and ω_{10}, the equation of motion of a single-mass mechanical system (1) was also solved using the third-order Hermite interpolation function. The result obtained in the form of a graph of a function $\omega_1(t)$ is overlaid on the graph obtained by the energy-mass method, which is traditional for the study of machines (Figure 9).

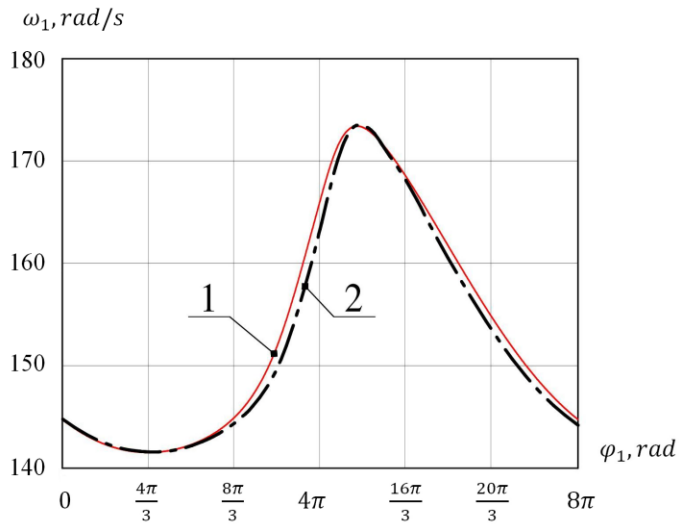

Figure 9. Graphs of function $\omega_1(\varphi_1)$ without flywheel: 1—the energy-mass method, 2—the third-order Hermite interpolation function.

It can be seen from the graph $\omega_1(\varphi_1)$ that the angular velocity of the reduction link is not a constant value and fluctuates around the average value. The velocity fluctuations are determined by the intra-cycle change in the gear ratio of the mechanism with elliptical gears. Irregularity of the initial link motion is characterized by the coefficient of rotation irregularity, which, in accordance with [42], is determined as:

$$\delta = \frac{\omega_{1max} - \omega_{1min}}{\omega_{av}}. \tag{27}$$

Preliminary calculations showed that the value of the irregularity coefficient exceeds the permissible value $[\delta] = 0.05$. Consequently, it is required to install a flywheel in the investigated actuator of the conveyor.

Flywheel moment of inertia I_f will be determined as:

$$I_f = \frac{C_{max} - C_{min}}{[\delta] \cdot \omega_{av}^2}. \tag{28}$$

After substitution in Equation (28) C_{max}, C_{min}, $[\delta]$ and ω_{av}, the required moment of inertia of the flywheel is obtained ($I_f = 0.01\ kg{\cdot}m^2$). Taking into account the flywheel installation, the angular velocity of the reduced link will be determined as:

$$\omega_1 = \sqrt{\frac{I_f{\cdot}\omega_{av}^2{\cdot}(1+[\delta]) - 2(C_{max} - \Delta T)}{I_f + I_r}}. \quad (29)$$

Using Equation (29) and the results of previous calculations, a graph of the function $\omega_1(\varphi_1)$ is constructed. The graph also shows the numerical solution of Equation (1) by the Hermite method, taking into account the moment of inertia of the flywheel (Figure 10).

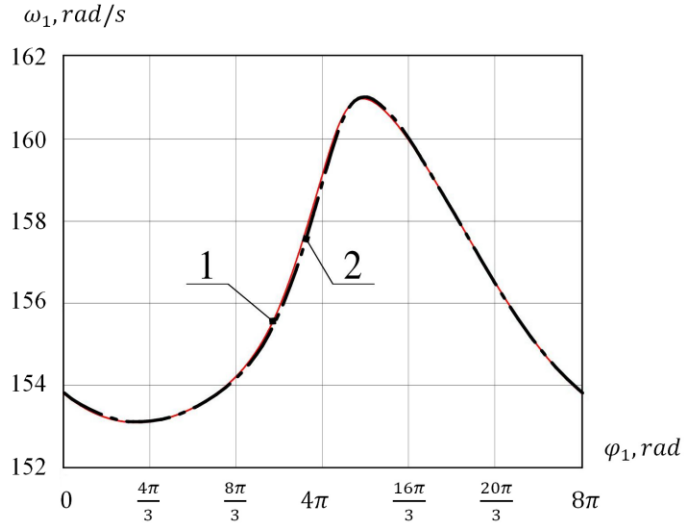

Figure 10. Graphs of function $\omega_1(\varphi_1)$ with flywheel: 1—the energy-mass method, 2—the third-order Hermite interpolation function.

As can be seen from the graphs, the installation of the flywheel made it possible to reduce rotation irregularity of the reduction link. The irregularity coefficient has decreased to the permissible value $[\delta] = 0.05$.

5. Conclusions

In the present study, a single-mass dynamic model of the intermittent-motion conveyor, the actuator of which is a planetary mechanism with elliptical gears, is constructed and investigated. Analysis of the presented mathematical model made it possible to highlight the following innovation results and conclusions:

- laws of motion of the reduction link (the input shaft of the mechanism) are obtained using the energy-mass method and the third-order Hermite interpolation function;
- analysis of the input link rotation irregularity is carried out;
- moment of inertia of the flywheel to reduce the irregularity coefficient is determined.

Studies have shown the convergence of the laws of motion obtained by various methods. The results of dynamic analysis can be used in the design and calculation of conveyors with the proposed planetary mechanism as part of the actuator.

Funding: This research was funded by scholarship of the president of the Russian Federation, grant number SP-2763.2019.1.

Institutional Review Board Statement: Not applicable.

Informed Consent Statement: Not applicable.

Data Availability Statement: Not applicable.

Conflicts of Interest: The author declares no conflict of interest.

References

1. Yao, Y.; Zhang, B. Influence of the elastic modulus of a conveyor belt on the power allocation of multi-drive conveyors. *PLoS ONE* **2020**, *15*, e0235768. [CrossRef] [PubMed]
2. Gao, R.; Miao, C.; Li, X. Adaptive multi-view image mosaic method for conveyor belt surface fault online detection. *Appl. Sci.* **2021**, *11*, 2564. [CrossRef]
3. Friso, D. Conveyor-belt dryers with tangential flow for food drying: Development of drying Odes useful to design and process adjustment. *Inventions* **2021**, *6*, 6. [CrossRef]
4. Dong, M.W.; Luo, Q. Research and application on energy saving of port belt conveyor. *Procedia Environ. Sci.* **2011**, *10*, 32–38. [CrossRef]
5. He, D.J.; Pang, Y.S.; Lodenijks, G. Green operations of belt conveyors by means of speed control. *Appl. Energy* **2017**, *188*, 330–341. [CrossRef]
6. Zimroz, R.; Krol, R. Failure analysis of belt conveyor systems for condition monitoring purposes. *Arch.Min. Sci.* **2009**, *128*, 255–270.
7. Andrejiova, M.; Grincova, A.; Marasova, D. Monitoring dynamic loading of conveyer belts by measuring local peak impact forces. *Measurement* **2020**, *158*, 107690. [CrossRef]
8. Draganová, K.; Semrád, K.; Spodniak, M.; Cúttová, M. Innovative analysis of the physical-mechanical properties of airport conveyor belts. *Transp. Res. Procedia* **2020**, *51*, 20–27. [CrossRef]
9. Bajda, M.; Hardygóra, M. Analysis of reasons for reduced strength of multiply conveyor belt splices. *Energies* **2021**, *14*, 1512. [CrossRef]
10. Trybała, P.; Blachowski, J.; Błazej, R.; Zimroz, R. Damage detection based on 3D point cloud data processing from laser scanning of conveyor belt surface. *Remote Sens.* **2021**, *13*, 55. [CrossRef]
11. Skoczylas, A.; Stefaniak, P.; Anufriiev, S.; Jachnik, B. Belt conveyors rollers diagnostics based on acoustic signal collected using autonomous legged inspection robot. *Appl. Sci.* **2021**, *11*, 2299. [CrossRef]
12. Gao, Y.; Qiao, T.; Zhang, H.; Yang, Y.; Pang, Y.; Wei, H. A contactless measuring speed system of belt conveyor based on machine vision and machine learning. *Measurement* **2019**, *139*, 127–133. [CrossRef]
13. Hou, C.; Qiao, T.; Zhang, H.; Pang, Y.; Xiong, X. Multispectral visual detection method for conveyor belt longitudinal tear. *Measurement* **2019**, *143*, 246–257. [CrossRef]
14. Zhang, M.; Zhou, M.; Shi, H. A computer vision-based real-time load perception method for belt conveyors. *Math. Probl. Eng.* **2020**, *2020*, 8816388. [CrossRef]
15. Che, J.; Qiao, T.; Yang, Y.; Zhang, H.; Pang, Y. Longitudinal tear detection method of conveyor belt based on audio-visual fusion. *Measurement* **2021**, *176*, 109152. [CrossRef]
16. Wodecki, J.; Zdunek, R.; Wyomańska, A.; Zimroz, R. Local fault detection of rolling element bearing components by spectrogram clustering with semi-binary NMF. *Diagnostyka* **2017**, *18*, 3–8.
17. Wodecki, J.; Michalak, A.; Zimroz, R.; Wyłomanska, A. Separation of multiple local-damage-related components from vibration data using nonnegative matrix factorization and multichannel data fusion. *Mech. Syst. Signal Process.* **2020**, *145*, 106954. [CrossRef]
18. Gładysiewicz, L.; Król, R.; Kisielewski, W. Measurements of loads on belt conveyor idlers operated in real conditions. *Measurement* **2019**, *134*, 336–344. [CrossRef]
19. Sclater, N.; Chironis, N.P. *Mechanisms and Mechanical Devices Sourcebook*; McGraw-Hill: New York, NY, USA, 2001.
20. Prikhodko, A.A. Experimental kinematic analysis of an intermittent motion planetary mechanism with elliptical gears. *J. Meas. Eng.* **2020**, *8*, 122–131. [CrossRef]
21. Sujan, V.A.; Meggiolaro, M.A. Dynamic optimization of Geneva mechanisms. In Proceedings of the International Conference on Gearing, Transmissions and Mechanical Systems, London, UK, 3–6 July 2000; pp. 687–696.
22. Lee, J.-J.; Jan, B.-H. Design of Geneva mechanisms with curved slots for non-undercutting manufacturing. *Mech. Mach. Theory* **2009**, *44*, 1192–1200. [CrossRef]
23. Kozhevnikov, S.N.; Esipenko, Y.I.; Raskin, Y.M. *Mechanisms*; Mechanical Engineering: Moscow, Russia, 1976.
24. Zheng, F.; Hua, L.; Han, X.; Li, B.; Chen, D. Synthesis of indexing mechanisms with non-circular gears. *Mech. Mach. Theory* **2016**, *105*, 108–128. [CrossRef]
25. Lin, C.; Xia, X.; Li, P. Geometric design and kinematics analysis of coplanar double internal meshing non-circular planetary gear train. *Adv. Mech. Eng.* **2018**, *10*, 1–12. [CrossRef]
26. Maláková, S.; Urbanský, M.; Fedorko, G.; Molnár, V.; Sivak, S. Design of geometrical parameters and kinematical characteristics of a non-circular gear transmission for given parameters. *Appl. Sci.* **2021**, *11*, 1000. [CrossRef]
27. Danieli, G.A.; Mundo, D. New developments in variable radius gears using constant pressure angle teeth. *Mech. Mach. Theory* **2005**, *40*, 203–217. [CrossRef]
28. Karpov, O.; Nosko, P.; Fil, P.; Nosko, O.; Olofsson, U. Prevention of resonance oscillations in gear mechanisms using non-circular gears. *Mech. Mach. Theory* **2017**, *114*, 1–10. [CrossRef]
29. Gao, N.; Meesap, C.; Wang, S.; Zhang, D. Parametric vibrations and instabilities of an elliptical gear pair. *J. Vib. Control* **2020**, *26*, 1721–1734. [CrossRef]

30. Liu, J.Y.; Chang, S.L.; Mundo, D. Study on the use of a non-circular gear train for the generation of Figure-8 patterns. *Proc. Inst. Mech. Eng. Part C* **2006**, *220*, 1229–1236. [CrossRef]
31. Prikhodko, A.A. Intermittent-motion planetary mechanism with elliptical gears. *Russ. Eng. Res.* **2020**, *40*, 1084–1086. [CrossRef]
32. Zheng, F.; Hua, L.; Han, X.; Li, B.; Chen, D. Linkage model and manufacturing process of shaping non-circular gears. *Mech. Mach. Theory* **2016**, *96*, 192–212. [CrossRef]
33. Sałacinski, T.; Przesmycki, A.; Chmielewski, T. Technological aspects in manufacturing of non-circular gears. *Appl. Sci.* **2020**, *10*, 3420. [CrossRef]
34. Wojtkowiak, D.; Talaska, K.; Wilczynski, D.; Górecki, J.; Wałesa, K. Determining the power consumption of the automatic device for belt perforation based on the dynamic model. *Energies* **2021**, *14*, 317. [CrossRef]
35. Prikhodko, A.A.; Smelyagin, A.I. Dynamic analysis of rotationally reciprocating stirred tank with multiple impellers. In Proceedings of the 2015 International Conference on Mechanical Engineering, Automation and Control Systems, Tomsk, Russia, 1–4 December 2015.
36. Braune, S.; Liu, S.; Mercorelli, P. Design and control of an electromagnetic valve actuator. In Proceedings of the 2006 IEEE Conference on Computer Aided Control System Design, 2006 IEEE International Conference on Control Applications, 2006 IEEE International Symposium on Intelligent Control, Munich, Germany, 4–6 October 2006.
37. Su, Y.; Zheng, C.; Mercorelli, P. Velocity-free friction compensation for motion systems with actuator constraint. *Syst. Signal Process.* **2021**, *148*, 107132. [CrossRef]
38. Liu, X.; Nagamura, K.; Ikejo, K. Analysis of the dynamic characteristics of elliptical gears. *J. Adv. Mech. Des. Syst. Manuf.* **2012**, *6*, 484–497. [CrossRef]
39. Cai, Z.; Lin, C. Dynamic model and analysis of nonlinear vibration characteristic of a curve-face gear drive. *J. Mech. Eng.* **2017**, *63*, 161–171. [CrossRef]
40. Zhao, Y.; Yu, G.H.; Wu, C.Y. Circuit Simulation and Dynamic Analysis of a Transplanting Mechanism with Planetary Elliptical Gears. *Trans. ASABE* **2011**, *54*, 1179–1188. [CrossRef]
41. Prikhodko, A.A.; Smelyagin, A.I. Balancing of the planetary actuator of the reciprocating stirring device. *Mech. Eng. Autom.* **2016**, *4*, 62–67. (In Russian)
42. Prikhodko, A.A.; Smelyagin, A.I. Dynamics of rotationally reciprocating stirred tank with planetary actuator. *J. Phys. Conf. Ser.* **2017**, *858*, 12026. [CrossRef]
43. Yazici, A.; Altas, I.; Ergenc, T. Symbolic polynomial interpolation using Mathematica. In *International Conference on Computational Science*; Springer: Berlin/Heidelberg, Germany, 2004; pp. 364–369.
44. Prikhodko, A.A. Structural and kinematic analysis of a stirred tank planetary drive. *MATEC Web Conf.* **2018**, *226*, 1012. [CrossRef]
45. Litvin, F.L.; Fuentes, A. *Gear Geometry and Applied Theory*, 2nd ed.; Cambridge University Press: Cambridge, UK, 2004.